Nanoscale

Accepted Manuscript

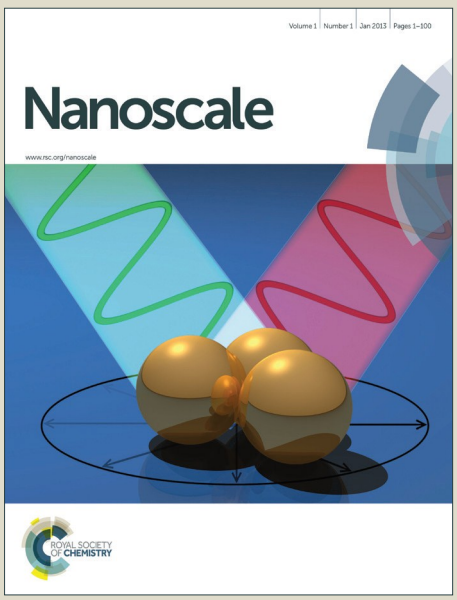

This is an *Accepted Manuscript*, which has been through the Royal Society of Chemistry peer review process and has been accepted for publication.

Accepted Manuscripts are published online shortly after acceptance, before technical editing, formatting and proof reading. Using this free service, authors can make their results available to the community, in citable form, before we publish the edited article. We will replace this *Accepted Manuscript* with the edited and formatted *Advance Article* as soon as it is available.

You can find more information about *Accepted Manuscripts* in the Information for Authors.

Please note that technical editing may introduce minor changes to the text and/or graphics, which may alter content. The journal's standard Terms & Conditions and the Ethical guidelines still apply. In no event shall the Royal Society of Chemistry be held responsible for any errors or omissions in this *Accepted Manuscript* or any consequences arising from the use of any information it contains.

ROYAL SOCIETY OF CHEMISTRY

www.rsc.org/nanoscale

Nanoscale

RSCPublishing

COMMUNICATION

Tuning the deposition of molecular graphene nanoribbons by surface functionalization

Cite this: DOI: 10.1039/x0xx00000x

R. Konnerth, [a] C. Cervetti,[a,b] A. Narita,[c] X. Feng,[c] K. Müllen,[c] A. Hoyer,[b,d] M. Burghard,[b] K. Kern,[b,d] M. Dressel[a] and L. Bogani[a,e]

Received 00th January 2012,
Accepted 00th January 2012

DOI: 10.1039/x0xx00000x

www.rsc.org/

We show that individual, isolated graphene nanoribbons, created with a molecular synthetic approach, can be assembled on functionalised wafer surfaces trated with silanes. The use of surface groups with different hydrofobicity allows tuning the density of the ribbons and assessing the products of the polymerisation process.

Graphene[1,2], a sheet of carbon atoms arranged in a hexagonal lattice, has attracted immense attention stimulated by both its fundamental properties and its application potential in range from nano-opto-electronics[3] to biosensors[4] and spintronics[5]. While most experiments have been performed using micrometer-size single flakes,[2] several proposals would require the creation of graphene ribbons with nanometer-size width (GNR)[6]. Perfect control over the width and edge geometry of GNRs might allow creating novel spintronic devices,[7] thermal rectifiers[8,9] and homogeneous graphene quantum dots.[10] A highly promising way of achieving such level of control is by a bottom-up synthetic approaches, i.e. by polymerising molecular units in a pre-determined pattern, followed by graphitisation. The first successful examples of this approach have only very recently appeared,[11-15] with the creation of the first molecular GNRs, which show atomically-regular edges over lengths of more than 500 nm. Such GNRs are an important breakthrough, allowing, for the first time, fine tuning of graphene nanostructures with the means and atomic precision of synthetic chemistry.

[a] 1. Physikalisches Institut, Universität Stuttgart, Pfaffenwaldring 57, D-70550, Stuttgart, Germany. E-mail: lapo.bogani@pi1.physik.uni-stuttgart.de

[b] Max Planck Institut für Festkörperforschung, Heisenbergstraße 1, D-70569 Stuttgart, Germany.

[c] Max Planck Institut für Polymerforschung, Ackermannweg 10, D-55128, Mainz, Germany.

[d] Institut de Physique de la Matière Condensée, Ecole Polytechnique de Lausanne, CH-1015, Lausanne, Switzerland.

[e] Department of Materials, University of Oxford, 16 Parks Road, OX1 3PH, Oxford, United Kingdom.

On the other hand, the assembly and organization of such GNRs, in conditions compatible with the creation of nanoelectronic devices, remains problematic[16]. This difficulty has so far prevented the exploitation of the full potential of molecular GNRs in nanoelectronics, and has hindered the observation of the predicted effects. Additionally, surface deposition would allow a statistical topographical analysis of the polymerisation reactions, necessary to test and improve the synthetic process and the possible presence of different sub-products.

In this Letter we address this problem by surface functionalization of commercial Si wafers to immobilize and isolate bottom-up synthesized GNRs on surfaces. The devised methodology compatible with the most widespread processes of nanoelectronic fabrication allows tuning the nanoribbons density by changing the surface hydrophobic character[17]. Moreover, we provide a full analysis of the depositions, extracting information on the polymerisation processes, on the surface interaction mechanisms and on the Raman signatures.

The GNRs here used are produced by bottom-up synthesis as previously reported[12] and have an atomically-defined edge structure, as shown in Figure 1a. Briefly, they are formed via AB-type Diels-Alder polymerization of monomeric units of 2,5-bis(4-dodecylphenyl)-3-(3-ethynylphenyl)-4-phenyl-2,4-cyclopentadienone, followed by graphitization into graphene nanoribbons via intramolecular oxidative cyclodehydrogenation. The structure of the synthetic GNRs, as obtained via multiple techniques,[12] is that of a flat, regular graphene strip, only 3-rings wide, with a "cove-type edge" structure containing dodecyl chains sprouting from it (Figure 1a). These side chains allow separating the ribbons and forming dispersions in organic solvents, such as N-Methyl-2-pyrrolidone or tetrahydrofurane, but do not introduce any degree of complexity and have almost no effect on the band structure.

In order to exploit the hydrophobicity of the GNRs for the deposition process, we functionalized the surfaces using different silanes (Figure 1b): (3-aminopropyl)triethoxysilane (APTES),

Nanoscale Accepted Manuscript

propyl-trimethoxysilane (Propyl-TMS), octyl-triethoxysilane (Ocyl-TES) and dodecyl-triethoxysilane (Dodecyl-TES). These four silanes promote, to a different degree, the deposition of hydrophobic materials via van der Waals interactions. Comparison is also performed with bare Si/SiO_2 wafer surfaces, which are terminated with hydrophilic -OH groups. The silanization (Figure 1c) was carried out by insertion of the wafer for 10 s in an aqueous dispersion of the silane, followed by cleaning in isopropanol. The GNRs were then deposited by casting 10 µl drops of a dispersion into N-Methyl-2-pyrrolidone[12] onto the substrates (Figure 1d).

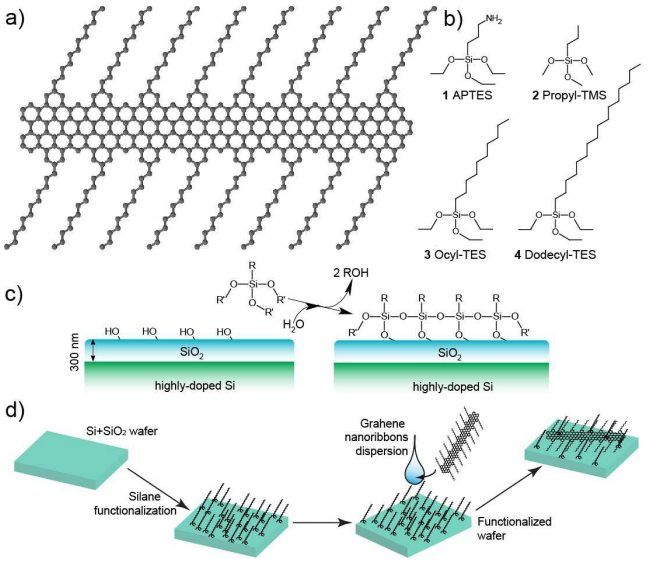

Fig. 1 (a) Molecular structure of the graphene nanoribbons. The ribbon structure is repeated regularly all over the length, with only a length distribution being present. (b) Chemical structures of the silanes used for the surface functionalization: **1,** (3-Aminopropyl)triethoxysilane, APTES; **2**, Propyl-trimethoxysilane, Propyl-TMS; **3**, Octyl-triethoxysilane, Octyl-TES; **4**, Dodecyl-triethoxysilane, Dodecyl-TES. (c) Scheme of the silane monolayer formation in the silanization reaction of SiO_2. (d) Scheme of the functionalization process. The wafer is first covered with functional silanes to alter the reaction properties, and then functionalized by drop casting using a dispersion of the molecular GNRs.

The resulting depositions were investigated using atomic force microscopy (AFM) in tapping mode (0.4 Hz, Olympus-3072 tips), as shown in Figure 2a. Under the employed deposition conditions, only a very few GNRs attach to the bare, untreated Si/SiO_2 surface, whereas numerous well-isolated ribbons can be observed on treated surfaces. The ribbons, although barely visible in the height topography, show an evident contrast in the phase and amplitude signals (Figures 2b and 2c), and always appear well-isolated. Even for exceptionally long ribbon lengths (see discussion below), the GNRs appear straight, in sharp contrast to the typical behaviour of carbon nanotubes, which have a strong tendency to coil and bundle on the surface. This behaviour is surprising, as theory predicts that GNRs to be more flexible than carbon nanotubes[18,19] and also contrasts with observations on top-down GNRs[20,21]. One possible explanation lies in a very pronounced interaction between the alkyl side chains of the GNRs and the functionalised surfaces, hindering folding and rolling up of the GNRs.

The AFM heights of most ribbons deposited on the functionalised surfaces are found to be around 7 Å (Figure 3a), in close correspondence with the well-established AFM height of monolayer graphene flakes on wafer surfaces[22]. The height of monolayer graphene derives largely from adsorbed water and hydrocarbons, and from chemical considerations, one could expect that the nanoribbons do not differ too much in their capacity of adsorbing such species, both above and below the ribbon. This agreement shows that the ribbons are not stacked one onto another, which may be a major issue with synthetically-obtained graphene analogues. The surface deposition of the ribbons thus meets all requirements for the fabrication of single-ribbon electronic nanodevices. The GNR widths are always found to be perfectly homogeneous, and correspond to

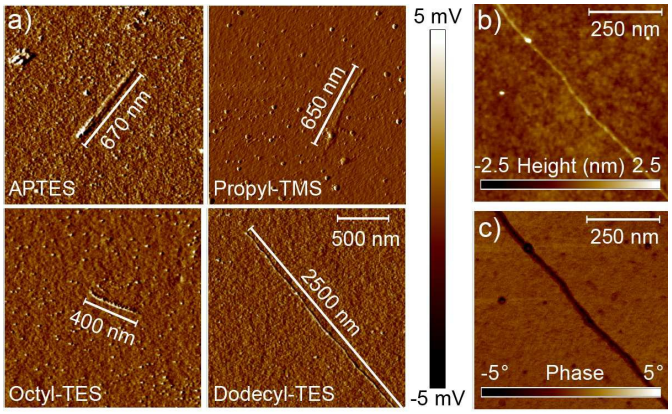

Fig. 2 (a) AFM amplitude images of the deposited molecular nanoribbons on surfaces functionalised with the different silanes. No ribbons were detected on bare wafer surfaces. (b) Small-area AFM topography of a ribbon deposited on Dodecyl-TMS, showing the details of the height profile. (c) AFM phase signal of a nanoribbon on the Dodecyl-TMS surface, showing the large phase contrast linked to the organic nature of the ribbon and its soft attachment to the surface.

the lateral AFM resolution, 7 nm, given by the AFM tip radius.

The GNR lengths were found to be similar in all samples, independent of the surface functionalization. For all different functionalisations, a bimodal gaussian distribution of lengths is always observed, with peaks at 400±20 and 620±20 nm (Figure 3b). This distribution matches the occurrence of two peaks in size-exclusion chromathography (SEC) analysis[12], performed on the polyphenylene precursor of the same GNRs sample employed in this study. The two peaks at different SEC retention times (Figure 3c) correspond, according to polystyrene standard calibration, to polymeric systems with masses of 360±100 kg/mol and 1000±250 kg/mol, where errors indicate the peak full-width-half-maxima. Such masses would indicate GNRs made of 510±120 and 1200±300 repeating units, which provide lengths of 350±100 and 900±250 nm, in reasonable agreement with the AFM distribution. The slight discrepancies between AFM and SEC analyses can be attributed to both the varying absorbances of the different polymer fractions in SEC (larger polymers have higher absorbance per polymer), along with the lower dispersibility and higher susceptibility to aggregation of longer GNRs. Our analysis thus confirms the formation of two preferential lengths, in the synthetic process[11], and excludes the creation of graphene nano-rings via head-to-tail cycloaddition during the

Nanoscale Accepted Manuscript

 This journal is © The Royal Society of Chemistry 2014

polymerisation step. In previous discussions, such rings were considered[12] as a plausible synthetic co-product.

While the ribbon length does not vary appreciably with surface functionalization, the surface density δ_s, given as the number of ribbons per square micron, changes considerably depending on the silane used. The distribution of the occurrence probability P_{δ_s} of the GNR densities were analysed with the quadrat method[23,24], choosing surface bins of 400 μm^2 (Figure 4a). The distributions show that an increasingly hydrophobic character of the surface results in a marked increase in the number of area units with larger δ_s. While no area unit has more than 2 GNRs for the bare SiO_2 surface, the Dodecyl-TES functionalization leads to 30% probability of having δ_s>3, with ca. 4% of the area units displaying up to 6 GNRs. The quadrat analysis also allows a rough assessment of the deposition process[24] via the parameter $\zeta = V_\delta/m$ (with V_δ the statistical variance in δ_s and m the mean value), which should be 1 for a random deposition, 0 for a regular arrangement and >>1 for clustered GNRs. The ζ values fall in the 1.2-1.6 range for all depositions, indicating slight clustering effects that become more pronounced on increasing the hydrophobic character of the surface (ζ=1.6 in Dodecyl-TES). This weak tendency to clustering, detectable also in the distributions of P_{δ_s} by the large remnant weight at δ_s=0, is attributable to small surface defects and bumps, which help local retention of the GNRs.

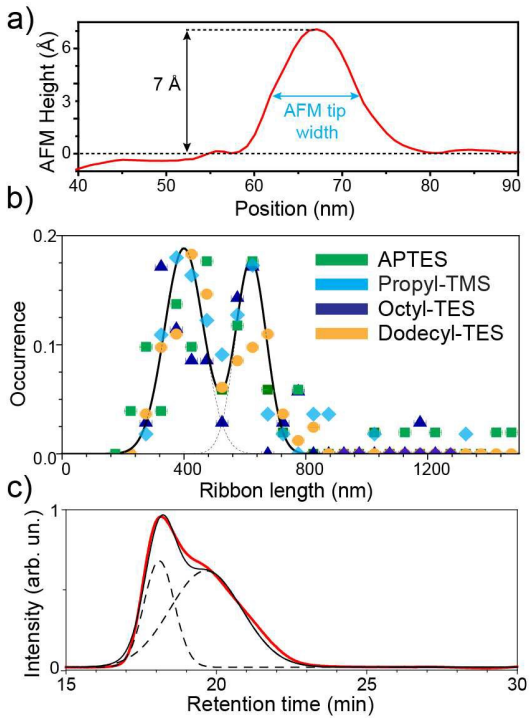

Fig. 3 (a) AFM height profile of a typical molecular nanoribbon, testifying the presence of only one graphitic layer; (b) Statistical analysis of the nanoribbon lengths observed with AFM, in dependence of the different surface functionalisation type. Lines are fits with a bimodal distribution (see text); (c) Size-exclusion chromatogram of the GNR precursor, after the Diels-Alder polymerisation and pre-graphitisation, showing the bimodal product distribution (eluent: THF; 1 mL/min; UV detector).

The importance of the surface-anchored groups is immediately detectable when considering the overall surface density $\Delta_r = \sum_{\delta_s} \delta_s P_{\delta_s}$, against the water contact angle, which is known from the literature and offers a good measure of the surface hydrophobicity. A clear correlation trend is observed (Figure 4b), when the length of the alkyl chain attached to the silane is increased, leading to a higher hydrophobicity of the surface. This non-covalent chemistry can already provide a more than four-fold enhancement of Δ_r from bare SiO_2 to the longest alkyl chain (Dodecyl-TES). The dependency is much stronger than for carbon nanotube depositions[25], and likely due to the decisive interaction with the ribbons dodecyl-side-chains.

Furthermore, we investigated the deposited ribbons using micro-Raman spectroscopy, which is one of the main tools for graphene characterization[26-29]. Graphene Raman spectra excited at 488 nm are characterized by a 2D peak around 2700 cm^{-1} and a G peak at 1585 cm^{-1}, plus additional D and D' peaks that correspond to Raman-

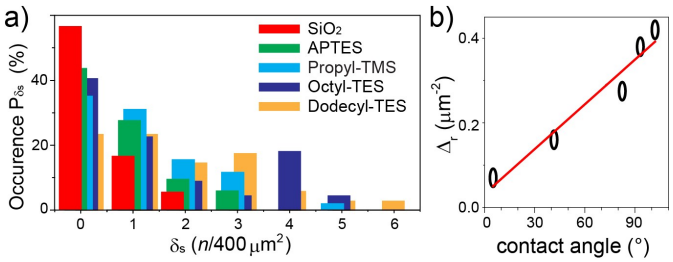

Fig. 4 (a) statistical distribution of the surface ribbon density, obtained from quadrat analysis of the differently-functionalized surfaces (see legend). The bars are slightly shifted horizontally to better show the evolution of the distributions. (b) Dependence of the surface ribbon density Δ_r on the surface hydrophobicity, measured as the water contact angle. Dot sizes correspond to estimated errors.

forbidden transitions, in a perfect graphene layer, and become activated by single-phonon inter-valley and intra-valley scattering processes, respectively. In GNRs the activation mechanisms are still unclear and await complete theoretical investigation, so that we only use the graphene peak labelling by analogy. Micro-Raman spectra of individual GNRs (Figure 5) clearly show all the aforementioned peaks, plus the D+D', G+D and 2D' overtone features, enabling precise peak determination even for slightly-overlapping G and D' peaks. G and 2D peaks are found at 1610 and 2675 cm^{-1}, respectively, and the deviations from graphene values can be attributed to lateral confinement effects[12], which are also responsible for the pronounced D and D' peaks appearing at 1348 and 1621 cm^{-1}, respectively[12,30]. The Raman spectra acquired on the liquid dispersions of the ribbons display the same features, with very similar relative intensities of the peaks, but considerable peak broadening and a 13 cm^{-1} downshift of the D peak are present, possibly linked to partial stacking in the dispersions[26-29]. The peaks of the ribbons in dispersion, contrarily to those of the deposited ribbons, could not be fitted with single Lorentzian lineshapes, but with Gaussian lines, indicating inhomogeneous broadening by sample averaging[31]. By comparison, the Raman spectrum of non-molecular ribbons (obtained by etching a 100-nm

Nanoscale Accepted Manuscript

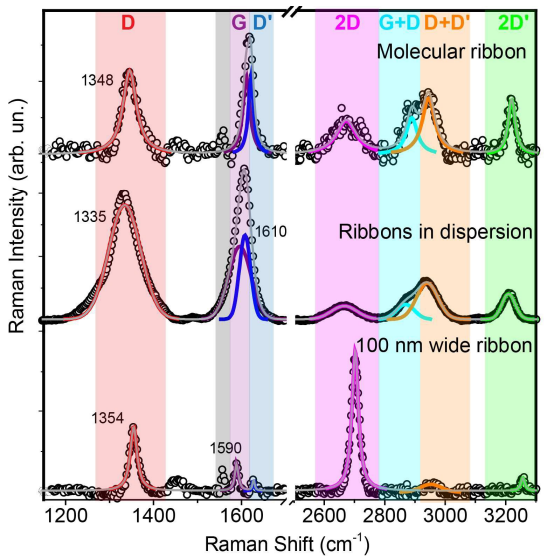

Fig. 5 Raman spectrum of an individual GNR on the Dodecyl-TES-functionalised surface (top) compared to the spectrum of a drop of the GNR in dispersion (middle) and to that of a 100-nm wide ribbon etched from exfoliated graphene by oxygen-plasma treatment (bottom). The lines are fits to the data (see text) while the colour bars highlight the different spectral regions.

wide patch from a single-layer exfoliated graphene flake via e-beam negative resist lithography) displays dominant D and 2D peaks, as well as D' and 2D' peaks whose intensity is only a fraction of the those of the GNRs.

Conclusions

We have demonstrated that silanization of Si/SiO_2 surfaces allows tuning the deposition of molecular graphene nanoribbon with atomically-precise edges. This opens up the possibility to fabricate large numbers of GNR-based nanoelectronic devices in parallel. Moreover, it enables a detailed statistical analysis of the ribbon structure, which is useful to identify strategies to further improve the synthesis protocol. Our analysis of the surface densities reveals that the deposition is influenced by van der Waals interactions between the ribbons and functionalized surface. GNR deposition differs remarkably from that of carbon nanotubes, for both the folding and the effect of the surface functionalization. The observations also shed new light on the nature of the synthetic products, and will prompt a better understanding of the chemical processes. Raman spectra of deposited ribbons show fingerprint features, not present in etched ribbons, which are promising to identify molecular ribbons. These findings pave the way to the detailed study of single molecular GNR and their use in nanoelectronics, and offer exciting perspectives for graphene spintronics.[27, 32]

Acknowledgments

We thank C. Casiraghi for insightful discussions and acknowledge financial support from German DFG, the BW-Stiftung (Kompetenznetz Funktionelle Nanostrukturen), the Royal Society via the University Research Fellowship, the AvH Stiftung (Sofja Kovalevskaja award), the IMPRS-AM and EU via the grants ERC-StG-338258-"OptoQMol", ERC-AdG-"NANOGRAPH", MoQuaS FP7-ICT-2013-10 and the EU Graphene Flagship (No. CNECT-ICT-604391).

References

1 A. H. Castro Neto, F. Guinea, N. M. R. Peres, K. S. Novoselov, and A. K. Geim, *Rev. Mod. Phys.*, 2009, **81**, 109.
2 A. K. Geim and K. S. Novoselov, *Nat. Mater.*, 2007, **6**, 183–191.
3 F. Bonaccorso, Z. Sun, T. Hasan, and A. C. Ferrari, *Nat. Photonics*, 2010, **4**, 611.
4 W. Yang, K. R. Ratinac, S. P. Ringer, P. Thordarson, J. J. Gooding, and F. Braet, *Angew. Chem. Int. Ed. Engl.*, 2010, **49**, 2114.
5 N. Tombros, C. Jozsa, M. Popinciuc, H. T. Jonkman and B. J. van Wees, *Nature*, 2007, **448**, 571.
6 P. Avouris, Z. Chen and V. Perebeinos, *Nature Nano.*, 2007, **2**, 605–615.
7 O. V. Yazyev, *Rep. Prog. Phys.*, 2010, **73**, 056501.
8 Y. Wang, A. Vallabhaneni, J. Hu, B. Qiu, Y. P. Chen and X. Ruan, *Nano Lett.*, 2014, **14**, 592–596.
9 J. Hu, X. Ruan and Y. P. Chen, *Nano Lett.*, 2009, **9**, 2730–2735.
10 B. Trauzettel, D. V. Bulaev, D. Loss and G. Burkard, *Nature Phys.* 2007, **3**, 192-196.
11 J. cai, P. Ruffieux, R. Jaafar, M. Bieri, T. Braun, S. Blankenburg, M. Muoth, A. P. Seitsonen, M. Saleh, X. Feng, K. Müllen and R. Fasel, *Nature*, 2010, **466**, 470-473.
12 A. Narita, X. Feng, Y. Hernandez, S. A. Jensen, M. Bonn, H. Yang, I. A. Verzhbitskiy, C. Casiraghi, M. R. Hansen, A. Koch, G. Fytas, O. Ivasenko, B. Li, K. Mali, T. Balandina, S. Mahesh, S. De Feyter and K. Müllen, *Nature Chem.*, 2014, **6**, 126-132.
13 A. N. Abbas, G. Liu, A. Narita, M. Orosco, X. Feng, K. Müllen and C. Zhou, *J. Am. Chem. Soc.*, 2014, **136**, 7555–7558.
14 T. H. Vo, M. Shekhirev, D. A. Kunkel, M. D. Morton, E. Berglund, L. Kong, P. M. Wilson, P. A. Dowben, A. Enders, A. Sinitskii, *Nature Comm.*, 2014, **5**, 3189.
15 N. Abdurakhmanova, N. Amsharow, S. Stepanow, M. Jansen, K. Kern, K. Amsharov, *Carbon* 2014, **77**, 1187.
16 P. B. Bennett, Z. Pedramrazi, A. Madani, Y.-C. Chen, D. G. de Oteyza, C. Chen, F. R. Fischer, M. F. Crommie, J. Bokor, *Appl. Phys. Lett.* 2013, **103**, 253114.
17 D. Janssen, R. De Palma, S. Verlaak, P. Heremans and W. Dehaen, *Thin Solid Films*, 2006, **515**, 1433-1438.
18 H. Pan, B. Chen, *Sci. Rep.*, 2014, **4**, 4198.
19 K. Bets, B. Yakobson, *Nano Res.*, 2009, **2**, 161.
20 X. Li, X. Wang, L. Zhang, S. Lee, H. Dai, *Science*, 2008, **319**, 1229.
21 L. Jiao, L. Zhang, X. Wang, G. Diankov, H. Dai, *Nature*, 2009, **458**, 877.
22 K. S. Novoselov, D. Jiang, F. Schedin, T. J. Booth, V. V. Khotkevich, S. V. Morozov and A. K. Geim, *Proc. Natl. Acad. Sci. U.S.A*, 2005, **102**, 10451-10453.
23 B. D. Ripley, *Spatial Statistics*, 2nd Ed. J. Wiley and Sons, Hoboken, New Jersey, 2004.
24 H. Solomon, Geometric Probability, SIAM, Philadelphia, 1978.

Nanoscale Accepted Manuscript

 This journal is © The Royal Society of Chemistry 2014

25 K. H. Choi, J. P. Bourgoin, S. Auvray, D. Esteve, G. S. Duesberg, S. Roth and M. Burghard, *Surf. Sci.*, 2000, **462**, 195-202, and references therein.
26 A. C. Ferrari, D. M. Basko, *Nature Nano*. 2013, **8**, 235–246.
27 M. S. Dresselhaus, A. Jorio, R. Saito, An. Rev. Cond. Mat. Phys. 2010, **1**, 89-108.
28 A. C. Ferrari, J. C. Meyer, V. Scardaci, C. Casiraghi, M. Lazzeri, F. Mauri, S. Piscanec, D, Jiang, K. S. Novoselov, S. Roth and A. K. Geim, *Phys. Rev. Lett.*, 2006, **97**, 187401.
29 C. Casiraghi, S. Pisana, K. S. Novoselov, A. K. Geim and A. C. Ferrari, *Appl. Phys. Lett.*, 2007, **91**, 233108.
30 S. Ryu, J. Maultzsch, M. Y. Han, P. Kim and L. E. Brus, *ACS Nano*, 2011, **5**, 4123-4130
31 P. G. Etchegoin and E. C. Le Ru, *Anal. Chem.*, 2010, **82**, 2888-2892.
32 C. Cervetti, E. Heintze, L. Bogani, *Dalton Trans.*, 2014, **43**, 4220–4232.

Nanoscale Accepted Manuscript